Design and Validation of a Detailed Aircraft Performance Model for Trajectory Optimization

William Camilleri[1]
Cranfield University, Cranfield, Bedford MK43 0AL, UK

Kenneth Chircop[2]
University of Malta, Msida, MSD 2080, Malta

David Zammit-Mangion[3]
University of Malta, Msida, MSD 2080, Malta
Cranfield University, Cranfield, Bedford MK43 0AL, UK

Roberto Sabatini [4] Vishal Sethi [5]
Cranfield University, Cranfield, Bedford MK43 0AL, UK

A key component in flight optimization studies is the aircraft performance model. This must be capable of representing to a high degree of fidelity the performance of the aircraft over its typical flight envelope if meaningful conclusions are to be made from the optimization studies. Flexibility is also required in order to facilitate robust trajectory definition and interoperability with secondary multidisciplinary tools. This paper describes the structure and main features of an Aircraft Performance Model (APM) specifically designed for use within a multi-disciplinary optimization environment. A validation exercise has been carried out against data generated with another aircraft performance model designed using the Base of Aircraft Data coefficients. Climb, cruise and descent phases have been investigated for the comparison. The performance of the aircraft predicted by the two models has been compared and found to compare well, with most cases resulting in less than a 0.5% mean variation between the two models.

Nomenclature

a	=	speed of sound
APM	=	aircraft performance model
AR	=	aspect ratio
ATM	=	Air Traffic Management
BADA	=	base of aircraft data
CAS	=	calibrated airspeed
CO_2	=	carbon dioxide
D	=	drag
ds	=	wing area due to flap extension
dt	=	time step
e	=	unit vector
EAS	=	equivalent airspeed
fsa	=	flap setting angle
h	=	altitude

[1] PhD Student, Department of Power and Propulsion
[2] Assistant Lecturer, Department of Electronic Systems Engineering, Member, AIAA.
[3] Associate Professor, Department of Electronic Systems Engineering / Lecturer in Avionics, Aerospace Engineering
[4] Lecturer in Avionics and CNS/ATM Systems, Aircraft Design Group, Department of Aerospace Engineering
[5] Research Fellow, Department of Power and Propulsion

ige	=	in ground effect
ITD	=	Integrated Technology Demonstrator
JTI	=	Joint Technology Initiative
L	=	lift
m	=	aircraft mass
M	=	Mach number
oge	=	out of ground effect
R	=	gas constant
S	=	surface area
sl	=	sea level
ssa	=	spoiler setting angle
SGO	=	Systems for Green Operations
TAS	=	true airspeed
WND	=	windspeed
wsa	=	wing setting angle
α	=	angle of attack
γ	=	flight path angle
ρ	=	density
η	=	specific fuel consumption
φ	=	bank angle
θ	=	pitch angle
ψ	=	heading angle
Λ	=	wing sweep

I. Introduction

The efficient management of a flight trajectory could contribute towards a reduction in mission block fuel burn, CO_2 and pollutant emissions, as well as a reduction in perceived noise levels at and around airports. Trajectory optimization has been the object of several recent studies, including the work in (1), (2) and (3). The Mission and Trajectory Management also forms a major study area within the Systems for Green Operations (SGO) Integrated Technology Demonstrator (ITD) in the European CleanSky Joint Technology Initiative (JTI). In this ITD, the identification of optimum trajectories based upon multiple criteria is sought. This involves multi-disciplinary simulation coupled with optimization to investigate multiple trajectories and to identify suitable solutions. A critical component in all such studies is the aircraft performance model which, simulates the dynamic performance of the aircraft in question. The model described in this work has been developed to model the performance of an Airbus A320 type aircraft.

The fundamental requirement for such a model is the correct representation of the behaviour of the aircraft, across its entire operational flight envelope. Although ground movement is also of interest, it is a diverse exercise from the traditional flight optimization towards which this exercise is geared. Beyond this requirement, the facility of trajectory definition and the flexibility of integration with multi-disciplinary model dependencies are also of strong significance. In the greater scope of this work, an optimization framework is used to automate the information exchange between different models (5). Within this context, the aircraft model must be capable of operating correctly with different user configurations and model input or output formats.

This paper outlines the structure and main features of an Aircraft Performance Model (APM) specifically designed for use within the said multi-disciplinary optimization environment. The model has been designed to address the main requirements of such an activity, namely validity and adaptability. The focus of this paper is the definition of the theoretical foundation of the model with special emphasis on the solution method. The second part of the paper addresses a validation activity which has been carried out against a second model. This latter model makes use of the data and methods contained with the base of aircraft data (BADA) which is widely acknowledged as the reference in Air Traffic Management (ATM) related work.

II. The Aircraft Performance Model

The APM is a quasi-steady-state model which is intended to characterize the dynamic airframe performance of an aircraft over a given flight segment. Specifically, it does not include engine performance, as this is considered an

external, separate model. Indeed, it is intended to work alongside other co-dependent models, such as engine performance models, combustor models and noise models, which, in unison, will represent the complete aircraft of interest and are able to determine a number of mission characteristics ranging from fuel burn to emissions. In the current applications of this model, the engine performance code has been supplied by Cranfield University (6) and is not considered as part of the aircraft performance tool. The main components of the APM are presented in Figure 1. The APM is used primarily to determine the control inputs required to achieve a given change of state or else to determine the change in state given pre-defined control inputs.

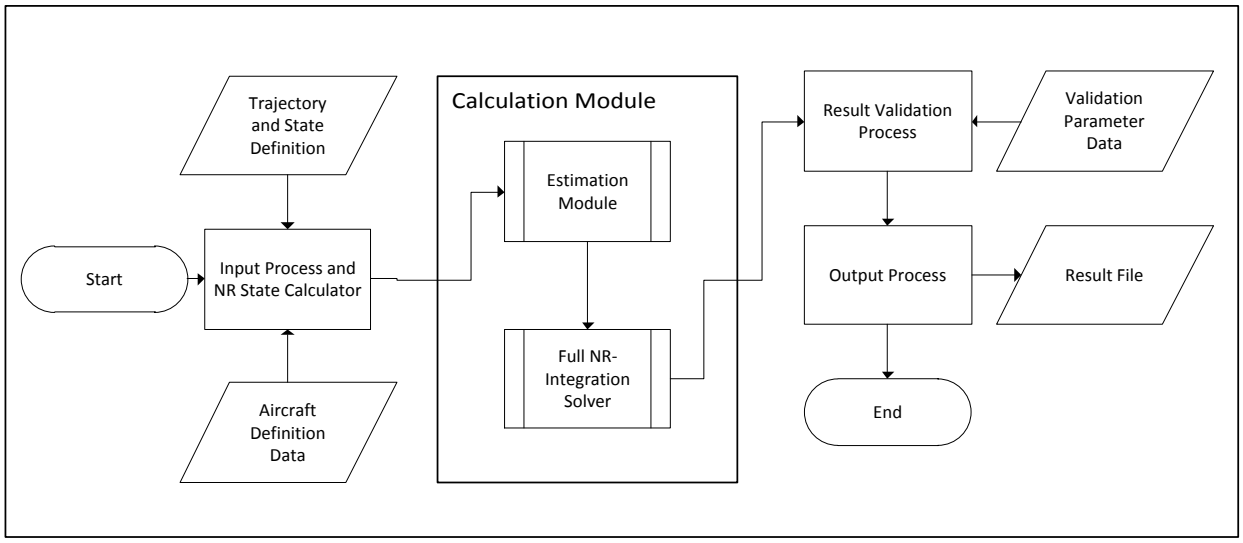

Figure 1 - APM process flowchart

The APM requires as inputs, the definition of the initial aircraft state specifically the position, mass and velocity as well as the wind vector. The flexibility of the model allows the user to provide vector inputs in a number of formats, such as orthogonal velocity vector components, resultant velocities, flight path angle, or heading angle. A multiroot newton-raphson (7), as shown in equation 5, or a broyden solver (8) is used to resolve all the remaining forms of velocity vectors. The reference velocity vector (Vref), with respect to ground, is iteratively modified in order to eliminate the difference between the user inputs and corresponding values calculated using equations 1-4. If a reference velocity is pre-defined, then the newton-raphson variable set is reduced.

$$\overrightarrow{V_{tas}} = \overrightarrow{V_{ref}} + \overrightarrow{V_{wnd}} \tag{1}$$

$$\overrightarrow{V_{eas}} = \overrightarrow{V_{tas}} \sqrt{\rho_{alt} / \rho_{msl}} \tag{2}$$

$$\overrightarrow{V_{mch}} = \overrightarrow{V_{tas}} \Big/ \sqrt{\gamma R T_s} \tag{3}$$

$$\overrightarrow{V_{cas}} = a_{sl} \sqrt{\left(\frac{2}{\gamma - 1}\right) + \vec{M}^2 - 1} \tag{4}$$

For a complete problem definition, the flight segment end-state or the control inputs of the flight segment must also be specified. The control inputs are defined as the thrust input, pitch angle, bank angle and flight time. Four independent parameters must be defined for the complete resolution of the problem. The segment characteristics are again determined using a multiroot newton-raphson or broyden solver. The control inputs are used as the algorithm variables. If a control is pre-defined the newton-raphson variable set is reduced.

$$\begin{bmatrix} \Delta V_1 \\ \vdots \\ \Delta V_n \end{bmatrix} = \begin{bmatrix} \frac{\partial E_1}{\partial V_1} & \cdots & \frac{\partial E_1}{\partial V_n} \\ \vdots & \ddots & \vdots \\ \frac{\partial E_n}{\partial V_1} & \cdots & \frac{\partial E_n}{\partial V_n} \end{bmatrix}^{-1} \times \begin{bmatrix} -E_1 \\ \vdots \\ -E_n \end{bmatrix} \tag{5}$$

Newton-Raphson root solution equation (7)

The problem can be solved in two ways. The first method assumes a linear transition between nodes. Therefore, the final state and/or controls are determined given the forces calculated only at the starting node. In the second method the flight time variable (dt) is used as the upper limit for an integration routine. The problem is then sub-divided into a number of discrete segments where the forces on the aircraft are re-calculated at each intermediate point. The difference between the two methods is significant as the linear method does not account for changing conditions between nodes. This limitation is critical when assuming large segments. The model solver operation is illustrated in Figure 2. The controls are maintained constant throughout each segment as updates requiring interaction with secondary models can only occur at nodes. The core of the calculation module is the aerodynamic force estimation together with the force resolution and state integration routines.

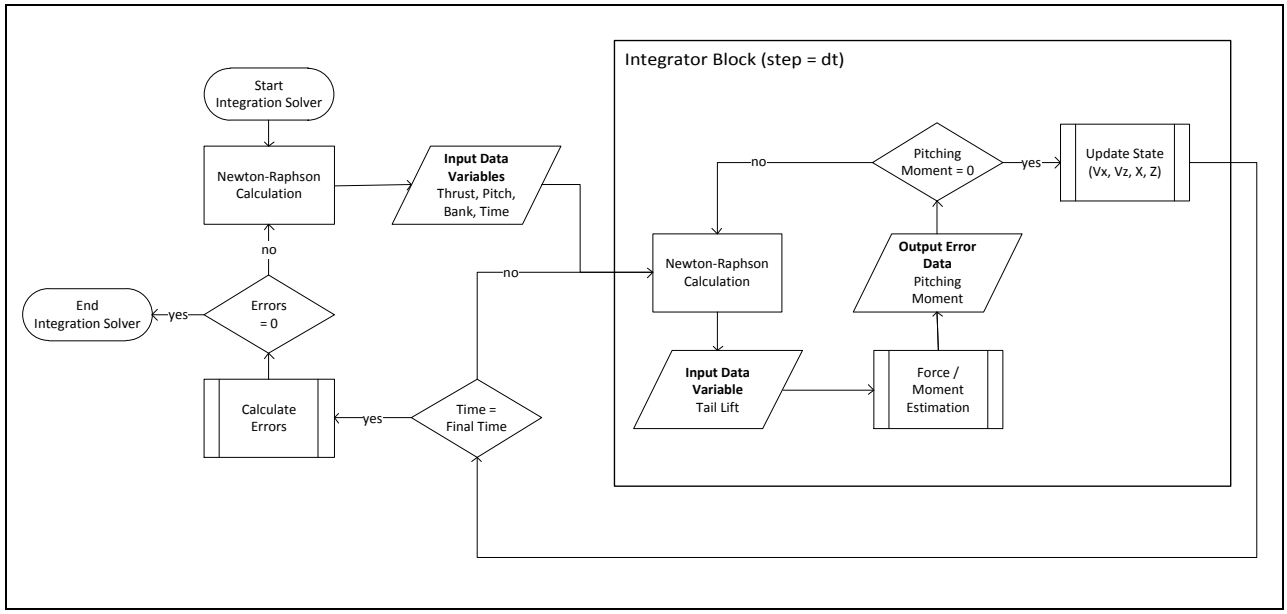

Figure 2 - Full Newton Raphson Solver

The aircraft is modelled as a rigid body consisting of two lifting surfaces, specifically the main wing and tail-plane. The model assumes complete freedom in terms of linear velocity and acceleration. Pitch and bank angles are assumed constant for each flight segment. Angular motion is not considered as the model does not aim to capture transient behaviours occurring over short periods. For the main wing, the lift (L) and drag (D) are determined according to the state and orientation of the aircraft using equations 6 and 7. The tail lift and drag are calculated using the same routine where the tail generated lift is determined using single root newton-raphson routine that adjusts the tail lift until the pitching moment due to all resultant forces on the aircraft is eliminated. The pitching moment must be zero in order to maintain angular equilibrium. The drag calculation is similar to that for the main wing except that the lift induced drag is determined from the resultant lift on the tail and not calculated from the aircraft state and orientation.

$$L = {}^{1}/_{2}\,\rho(S + dS){V_{tas}}^{2}C_L \tag{6}$$

$$D = {}^{1}/_{2}\,\rho(S + dS){V_{tas}}^{2}C_D \tag{7}$$

The lift coefficient (C_L) for the main wing is made up of four separate components; the lift coefficient at zero angle of attack (C_{L0}) and lift-coefficient increments dCl_{α}, dCl_{flaps} and $dCl_{spoiler}$. The lift-curve slope, used to determine $dC_{l\alpha}$, is calculated using equation (8) from reference (9). This relationship takes into account the effects of aspect ratio, sweep and compressibility. The change in lift-coefficient with flap setting angle derivatives ($dC_L/dfsa$) are currently user defined inputs. Currently the specific flap setting is selected by the user. However it can be selected according to flight speed if necessary. The change in lift-coefficient with spoiler setting angle derivatives ($dC_L/dssa$) derivative is currently also user defined. The coefficients are aircraft specific and flight phase specific and must be adjusted based on mean conditions. Any number of coefficient sets corresponding to different flight phases can be used. The spoiler angle is used as a variable in the newton-raphson routine in place of the thrust setting if the thrust requirement falls below a predefined minimum thrust level.

$$\frac{dC_L}{d\alpha} = \frac{2\pi AR}{2+\left((4+AR^2).(1-M^2+tan^2\,\Lambda)\right)} \tag{8}$$

$$C_L = C_{Lo} + (\alpha + wsa)\frac{dC_L}{d\alpha} + fsa.\frac{dC_L}{dfsa} + ssa.\frac{dC_L}{dssa} \tag{9}$$

The drag coefficient for both the tail and main wing are made up of two components, namely the zero lift drag and the lift-induced drag. The zero lift drag coefficient (C_{do}), defined by the user, is referred to the wing area but is representative of the entire aircraft body. A description of the drag polar as implemented here can be found in (10). The lift-induced drag coefficient (Cdi) is determined by equation 10. A correction to the induced drag is also made to account for the ground effect as can be seen in equation 11.

$$C_{Di_{oge}} = \frac{(C_L - C_{Lo})^2}{\pi.AR.e} \tag{10}$$

$$C_{Di_{ige}} = C_{Di_{oge}}\left[\frac{(16h/b)^2}{1+(16h/b)^2}\right] \tag{11}$$

$$C_D = C_{Do} + C_{Di_{ige}} \tag{12}$$

In addition to aerodynamic forces and moments, the system includes the forces and moments brought about by the powerplant (thrust) and weight. The aerodynamic forces are calculated in the wind axes, weight in the inertial axes while thrust acts along the powerplant centreline axis. These are first resolved into the aircraft body axis using the direction cosine matrix (D) in equation 14. The total force is then resolved in the earth reference axis. In equation 14, ψ is ignored as currently only vertical profiles have been considered.

$$D(\phi,\theta,\psi) = \begin{bmatrix} \cos\theta\cos\psi & \cos\theta\sin\psi & -\sin\theta \\ \sin\phi\sin\theta\cos\psi - \cos\phi\sin\psi & \sin\phi\sin\theta\sin\psi + \cos\phi\cos\psi & \sin\phi\cos\theta \\ \cos\phi\sin\theta\cos\psi + \sin\phi\sin\psi & \cos\phi\sin\theta\sin\psi - \sin\phi\cos\psi & \cos\phi\cos\theta \end{bmatrix} \tag{13}$$

$$\overrightarrow{F_{body}} = D(\phi,\theta,0).\overrightarrow{F_{mg}} + D(0,\alpha+wsa,0).\overrightarrow{F_{wing}} + D(0,\alpha,0).\overrightarrow{F_{tail}} + D(0,tilt,0).\overrightarrow{F_{eng}} \tag{14}$$

$$\overrightarrow{F_{ref}} = D\left(\phi_{ref},\theta_{ref},\psi_{ref}\right).\overrightarrow{F_{body}} \tag{15}$$

The resolved total force is then used to determine the acceleration of the aircraft. As the model assumes no rotational velocity or acceleration, the kinematic equations of motion reduce to equations 16-18.

$$r\hat{e} = x\hat{\imath} + y\hat{\jmath} + z\hat{k} \tag{16}$$

$$(r.\hat{e})_{n+1} = (r.\hat{e})_n + (\dot{r}.\hat{e})_n dt + 0.5(\ddot{r}\hat{e})_n dt^2 \tag{17}$$

$$(\dot{r}\hat{e})_{n+1} = (\dot{r}\hat{e})_n + (\ddot{r}\hat{e})_n dt \tag{18}$$

III. The BADA Aircraft Performance Model

Validation of the model is of paramount importance as it is necessary to ensure that trajectories generated using the APM represent, to a high level of fidelity, the behaviour of the real aircraft. Since public domain aircraft performance data is not readily available, a simple state-space aircraft performance model designed using Base of Aircraft Data (BADA) (11) coefficients was used for model validation purposes. BADA is developed and maintained by EUROCONTROL through active cooperation with aircraft manufacturers and operating airlines. It is developed for use in aircraft trajectory simulations and predictions in air traffic modelling and simulation tools, ground based operational Air Traffic Management (ATM) systems and environmental studies, amongst other applications. BADA is made out of two components, namely the model specifications and the datasets. The former are provided in the form of generic polynomial expressions used to calculate aircraft performance parameters based on the Total Energy Model (TEM) in which the rate of work done by the forces acting on the aircraft are equated to the rate of increase in potential and kinetic energy (12). The latter is a dataset specific to a large number of aircraft with coefficients present in the model specification. In this work the dataset corresponding to an Airbus A320 aircraft fitted with CFM 56 engines were used. The first-order differential equations were developed based on the work of Glover and Lygeros (13).

The states of the model are the horizontal positions X and Y, the altitude (h), the true airspeed (TAS), the flight path angle γ and the heading angle ψ. The control inputs to the model are the engine thrust T, the angle of attack α and the bank angle φ. Assuming a point mass model in still air conditions, the resulting equations of motion are the following:

$$\dot{X} = V\cos(\psi)\cos(\gamma) \tag{19}$$

$$\dot{Y} = V\sin(\psi)\cos(\gamma) \tag{20}$$

$$\dot{h} = V\sin\gamma \tag{21}$$

$$\dot{V} = \frac{1}{m}[(T\cos(\alpha) - D) - mg\sin(\gamma)] \tag{22}$$

$$\dot{\psi} = \frac{1}{mV}(L\sin(\varphi) + T\sin(\alpha)\sin(\varphi)) \tag{23}$$

$$\dot{\gamma} = \frac{1}{mV}[(L + T\sin(\alpha))\cos(\varphi) - mg\cos(\gamma)] \tag{24}$$

where m is the mass of the aircraft and g the gravitational acceleration. The lift and drag forces, L and D respectively, are calculated using BADA coefficients as follows:

$$L = \frac{1}{2}C_L\rho V^2 S \tag{25}$$

$$D = \frac{1}{2}C_D\rho V^2 S \tag{26}$$

where, the lift coefficient C_L, is determined assuming the flight path angle is zero but with a correction for the bank angle φ:

$$C_L = \frac{2mg}{\rho V^2 S\cos\varphi} \tag{27}$$

The drag coefficient, C_D is calculated as a function of the lift coefficient C_L. Equation 28 is valid for all configurations except for the approach and landing where other drag coefficients are used to model the different flap settings. Equations 29 and 30 are used for the approach and landing respectively:

$$C_D = C_{D0,CR} + C_{D2,CR}C_L^2 \tag{28}$$

$$C_D = C_{D0,AP} + C_{D2,AP}C_L^2 \tag{29}$$

$$C_D = C_{D0,LDG} + C_{D0,\Delta LDG} + C_{D2,LDG}C_L^2 \tag{30}$$

where $C_{D0,CR}$, $C_{D2,CR}$, $C_{D0,AP}$, $C_{D2,AP}$, $C_{D0,LDG}$, $C_{D0,\Delta LDG}$ and $C_{D2,LDG}$ are the BADA (12) drag coefficients that are specific to the aircraft type.

The area of application of the model is specifically trajectory optimization of commercial airliners. Thus, the model can be further simplified by assuming that the aircraft operates in trimmed flight conditions and at constant low angle of attack, and by treating the flight path angle as a control input instead of a state. An additional state is also included to model the changing mass of the aircraft due to fuel consumption. Applying these changes, the resulting model is made up of six states (X, Y, h, V, ψ, m) and three control inputs (T, γ) :

$$\dot{X} = V\cos(\psi)\cos(\gamma) \tag{31}$$

$$\dot{Y} = V sin(\psi)\cos(\gamma) \tag{32}$$

$$\dot{h} = V\sin(\gamma) \tag{33}$$

$$\dot{V} = -\frac{C_D S\rho V^2}{2m} - g\sin(\gamma) + \frac{T}{m} \tag{34}$$

$$\dot{\psi} = \frac{C_L S\rho V}{2m}\sin(\psi) \tag{35}$$

$$\dot{m} = -f \tag{36}$$

where f is the nominal fuel flow which is calculated as a function of thrust T and thrust specific fuel consumption η. The latter is specified as a function of true airspeed V and the fuel consumption coefficients C_{f1} and C_{f2}:

$$\eta = C_{f1}\left(1 + \frac{V}{C_{f2}}\right) \tag{37}$$

$$f = \eta T \tag{38}$$

Equation 38 is valid for all flight phases except during idle descent and cruise, in which equations 39 and 40 are used respectively and incorporate different fuel consumption coefficients, namely, C_{f3}, C_{f4} and C_{fcr} (12):

$$f = C_{f3}\left(1 - \frac{h}{C_{f4}}\right) \tag{39}$$

$$f = \eta T C_{fcr} \tag{40}$$

In the context of the work presented in this paper, flight trajectory optimization is only performed in the vertical profile. Moreover, the thrust control input is replaced by a thrust ratio TR, which is a function of the maximum thrust provided by the engines at a particular altitude, T_{max}, such that:

$$TR = \frac{T}{T_{max}} \tag{41}$$

$$T_{max} = C_{Tc,1}\left(1 - \frac{h}{C_{Tc,2}} + C_{Tc,3}h^2\right) \tag{42}$$

$C_{Tc,1}$, $C_{Tc,2}$, and $C_{Tc,3}$ are engine thrust coefficients. The value of T_{max} assumes standard atmospheric conditions, with corrections required for temperature deviations. Moreover, T_{max} is the absolute maximum thrust which is also degraded for prolonged flight times, such as in the cruising phase of flight. The final model is represented with four states (X, h, V, m) and two control inputs (TR, γ) as follows:

$$\dot{X} = V\cos(\gamma) \tag{43}$$

$$\dot{h} = V\sin(\gamma) \tag{44}$$

$$\dot{V} = -\frac{C_D S\rho V^2}{2m} - g\sin(\gamma) + \frac{(T_{max})(TR)}{m} \tag{45}$$

$$\dot{m} = -f \tag{46}$$

IV. Comparison of the APM with the BADA model

Three profiles for each of the climb, cruise and descent flight phases were considered in this comparison. The said flight phases were considered to be the major areas of interest during trajectory optimization and therefore a high level of fidelity of any model during these phases is critical. Three arbitrary trajectories, one per phase, were generated using the BADA model. In each case, the initial condition of the aircraft, including weight, TAS, flight path angle and position, were defined. The initial state was integrated with a one second timestep. The flight path angle and thrust were also defined for each timestep. The outcome of the integration routine is the final position and velocity of the aircraft. The same setup including initial conditions and control values were used in the APM and the resultant trajectories compared accordingly.

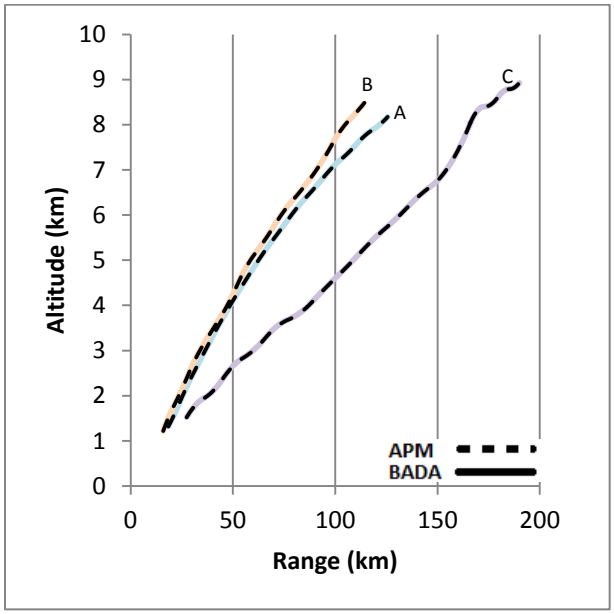

Figure 3 – Climb Altitude vs. Range

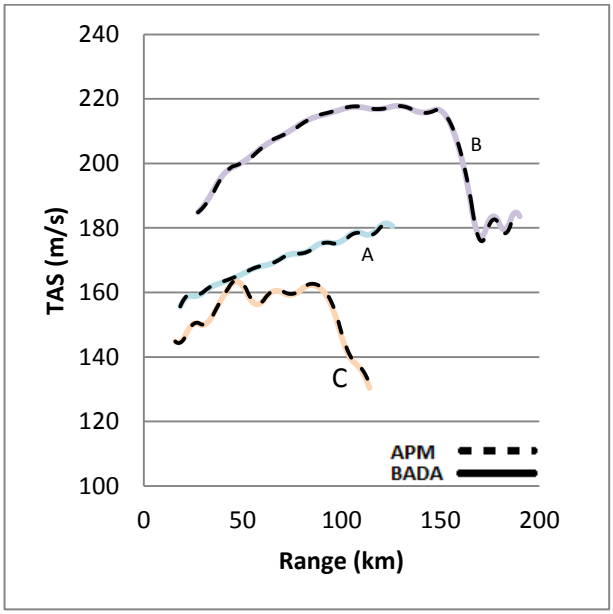

Figure 4 – Climb TAS vs. Range

	Mean (%)			Standard Deviation			Maximum (%)		
	A	**B**	**C**	**A**	**B**	**C**	**A**	**B**	**C**
X	0.06	-0.02	0.06	0.03	0.02	0.07	0.01	-0.06	0.17
Z	0.05	-0.07	-0.02	0.04	0.07	0.08	0.14	-0.28	-0.19
TAS	0.00	-0.09	0.21	0.13	0.29	0.24	0.32	-1.06	0.82

Table 1 – Discrepancy in Climb Results between APM and BADA model

Figure 3 and Figure 4 show the results from the three climb cases. The predicted trajectories from the APM are superimposed on the results of the BADA model. Figure 3 shows the climb profiles while Figure 4 shows the speed schedules. In both figures it is evident that the models predict practically the same trajectory given the same control set. This can be seen in Table 1, the standard deviation in the percentage variation of the APM results from the BADA data is minimal.

It is interesting to note that the greatest error occurs in the predicted TAS with case B showing a maximum variation of up to -1.06%. Both models predict acceleration based upon the resolution of forces acting on the aircraft. Any difference in this estimate will have a greater effect upon TAS prediction then on position as can be seen from equations 17-18. This is reflected in Table 1.

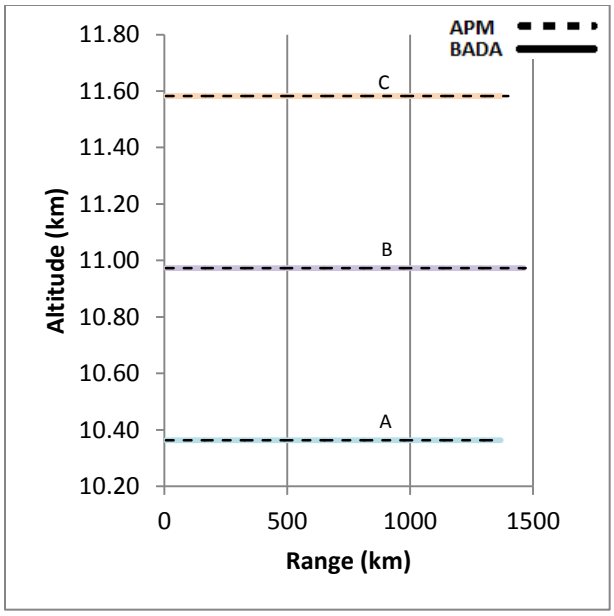

Figure 5 – Cruise Altitude vs. Range

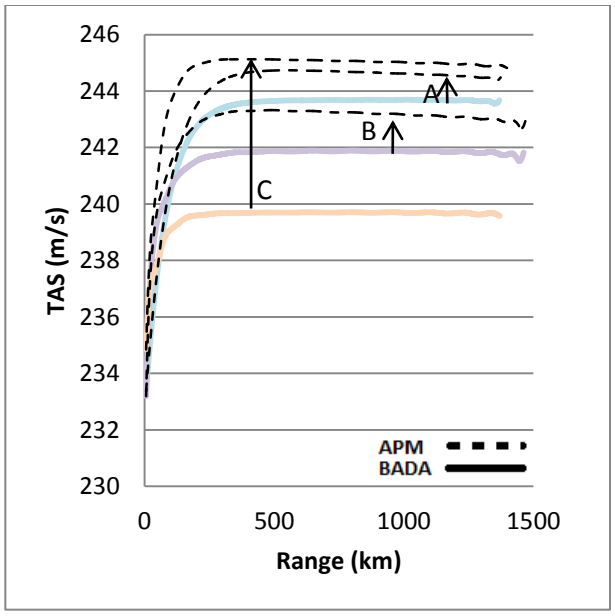

Figure 6 – Cruise TAS vs. Range

	Mean (%)			Standard Deviation			Maximum (%)		
	A	**B**	**C**	**A**	**B**	**C**	**A**	**B**	**C**
X	0.28	0.45	1.90	0.11	0.12	0.41	0.36	0.52	2.14
Z	0.00	0.00	0.00	0.00	0.00	0.00	0.00	0.00	0.00
TAS	0.36	0.52	2.15	0.10	0.10	0.30	0.44	0.60	2.27

Table 2– Discrepancy in Cruise Results between APM and BADA model

Figure 5 and Figure 6 show the results from the three cruise cases. The predicted trajectories from the APM are again superimposed on the results of the BADA model. In this flight phase an appreciable difference between the results of the two models is observed. It is clear from Figure 6 that the APM predicts an overall higher TAS then the BADA model. This is more pronounced at lower altitudes. To understand the reason for this variance one must assess the lift equation (8) used in the APM. In this model, unlike in BADA, a correction for Mach effects is made to the lift-curve slope, which leads to a steeper gradient for a given Mach number. The increase in lift coefficient, at a given angle of attack, necessitates a reduction in θ for level flight at a given flight condition, leading, consequently, to a slight increase in velocity. As altitude increases, this effect is more pronounced, as for a given TAS the Mach number will increase. It must be pointed out that, in reality, wave drag, which is not considered, would also increase in the transonic regime. Although the scale of this increase is considered small, the effect would offset the increase in velocity seen here, for a given thrust, as drag would rise.

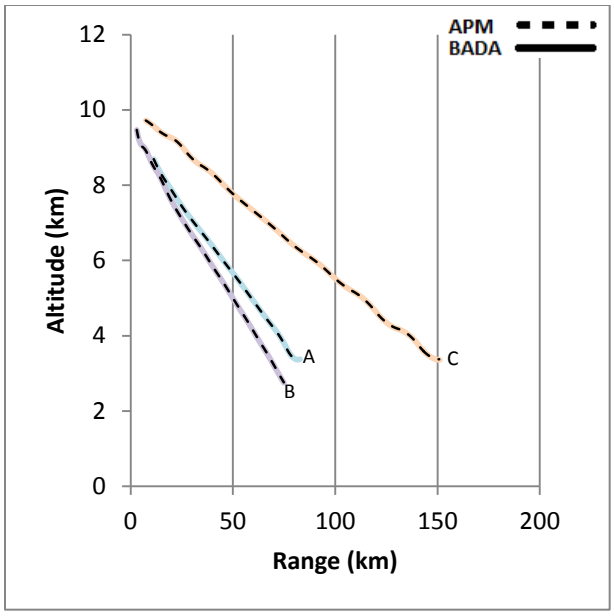

Figure 7 – Descent Altitude vs. Range

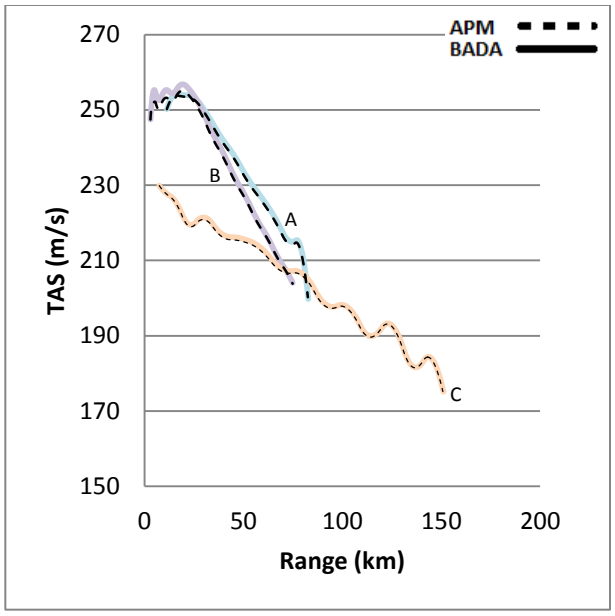

Figure 8 – Descent TAS vs. Range

	Mean (%)			Standard Deviation			Maximum (%)		
	A	**B**	**C**	**A**	**B**	**C**	**A**	**B**	**C**
X	-0.17	0.00	-0.20	0.08	0.00	0.06	-0.26	0.00	-0.25
Z	0.05	0.03	0.15	0.10	0.17	0.12	0.33	-0.31	0.48
TAS	-0.27	-0.47	-0.19	0.10	0.25	0.11	-0.31	-1.25	0.04

Table 3 - Variation in Cruise Results between APM and BADA model

Finally Figure 7 and Figure 8 show the results from the three descent cases where the predicted trajectory from the APM are superimposed on the results of the BADA model. As for the cruise and, to a greater extent the climb, good agreement has been obtained between the two models for all three descent profiles. It must be pointed out that the BADA model assumes that no spoilers are needed to aid the descent of the aircraft. While the APM contains spoiler routines, these were not used for this particular study.

V. Conclusion and Future Work

This paper described in detail the validity of the APM within the confines of its typical current usage. Within these confines, a number of potential key improvements may exist. Firstly, a more detailed drag estimation procedure could be implemented. The current algorithm does not take into account wave drag, leading to inaccuracies in the transonic regime, and this too could be modelled for greater accuracy.

Currently, APM has only been used for vertical trajectories. However, the model has been designed to support trajectory studies in 3D and 4D environments. Further development may therefore include expansion of the aerodynamic model to include the effects of turning flight. Furthermore, the inclusion of modelling ground manoeuvres is under consideration.

The APM model described here has been compared with a typical BADA model implementation and was found to agree well. The mean variance between the results is well below 0.5% in most cases. The cruise phase shows the greatest differences from the BADA results. The mean difference in TAS here reaches 2.15% for a high altitude cruise which is attributed to an aircraft pitch that varies at different Mach numbers for a given condition. Further investigation of the influence of the lift-curve slope Mach correction factor is warranted. The inclusion of further Mach related effects is to be considered for future releases.

Acknowledgments

The research leading to these results has received funding from the European Union's Seventh Framework Programme (FP7/2007-2013) for the Clean Sky Joint Technology Initiative under grant agreement n° CSJU-GAM-SGO-2008-001.

References

[1] M.C., Bartholomew-Biggs, Parkhurst, S.C. and Wilson, S.P "Global optimization approaches to an aircraft routing problem" *European Journal of Operational Research 2003*

[2] Sridhar, B., Ng, H.K. and Chen, N.Y. "Aircraft trajectory optimization and contrails avoidance in the presence of wind", *AIAA Aviation Technology, Integration, and Operation Conference 2010.*

[3] Chircop, Kenneth, et al., "Multi-Objective Optimisation of a constrained 2000km Trajectory using Genetic Algorithm" *CEAS 2011*

[4] CleanSky SGO ITD Website . 31 May 2012. http://www.cleansky.eu/content/project/system-green-operations.

[5] Chircop, Kenneth, et al., "A Generic Framework For Multi-Parameter Optimisation of FlightT Trajectories" *ICAS 2010.*

[6] Pervier, Hugo, et al., "Application of Genetic Algorithm for Preliminary Trajectory Optimization*" November 2011 SAE International Journal of Aerospace*, Vols. 4:973-987.

[7] Kurzke, Joachim. *GasTurb 11 Manual*. 2011.

[8] Press, William H., et al., *Numerical Recipes in C++: The Art of Scientific Computing*. Cambridge University Press, 2002.

[9] Ojha, Shiva Kumar. "Flight Performance of Aircraft" *American Institute of Aeronautics and Astronautics*, 1995. ISBN: 1563471132 .

[10] Asselin, Mario. "An Introduction to Aircraft Performance" *American Institute of Aeronautics and Astronautics*, 1997. ISBN: 9781563472213.

[11] Eurocontrol Website http://www.eurocontrol.int/products/bada.

[12] User Manual for the Base of Aircraft Data, version 3.7. s.l. : Eurocontrol, 2009.

[13] Glover, W. and Lygeros, J. "A Multi-Aircraft Model for Conflict Detection and Resolution Algorithm Evaluation" *Technical Report WP1, Deliverable D1.3, Version 1.3. HYBRIDGE :* s.n., February 18, 2004.

[14] Cook, Michael V. "Flight Dynamics Principles, Second Edition*" Butterworth-Heinemann, 2007.*